JOURNAL OF AIRCRAFT
Vol. 42, No. 3, May–June 2005

Computational Study of the Abrupt-Wing-Stall Characteristics of F/A-18E and F-16C

Paresh Parikh*
NASA Langley Research Center, Hampton, Virginia 23681-2199
and
James Chung†
U.S. Naval Air Systems Command, Patuxent River, Maryland 20670

Steady-state computational-fluid-dynamic (CFD) simulations are used to gain an understanding of the physics behind the abrupt-wing-stall (AWS) phenomenon and to arrive at static figures of merit (FOMs). Navier–Stokes solutions are obtained using the NASA Langley Research Center developed TetrUSS simulation suite, which is based on tetrahedral, unstructured grids. The physics of the AWS phenomenon is understood by comparing CFD simulation results on two aircraft; a preproduction F/A-18E configuration, which exhibits AWS phenomenon under certain geometric and flow conditions, and an F-16C aircraft configuration that does not. The computational results are used to understand the possible causes of AWS by comparing the detailed flowfields between the two configurations under a variety of flow conditions. Based on this approach, a number of static figures of merit are developed to predict AWS. The potential FOMs include the break in the lift and wing-root bending moment vs angle of attack α and the rate of change of sectional lift with respect to α. A companion paper describes a similar study for the AV-8B Harrier and F/A-18C.

Introduction

ABRUPT wing stall (AWS) is the uncommanded lateral-directional motion experienced by an aircraft during transonic maneuvering conditions. One of the aims of the joint NASA/Navy/Air Force AWS Program was to understand the physical flow mechanism responsible for the phenomenon. Such an understanding can then be used to arrive at guidelines with which to evaluate any new aerospace design for the likelihood of AWS and, if found, to fix the problem in the early design phase.

The program contained an extensive and complementary combination of experimental and computational studies, both steady and unsteady, to accomplish this aim. These studies were designed to learn the physics behind the AWS phenomenon by comparing and contrasting data on configurations that did and did not show AWS tendencies in flight. The aircraft configurations studied included a preproduction F/A-18E and AV-8B, both showing AWS when flown at a certain combination of geometric and flow conditions. Results of these two configurations were compared with similar results for the F-16C and F/A-18C, both of which do not exhibit AWS in their normal operational regime.

The present study is the first of a two-part computational-fluid-dynamics (CFD) study complementing the static wind-tunnel tests conducted during the AWS program. Each part compares and contrasts one aircraft configuration that exhibits AWS and one that does not. Both of these studies were conducted using a high-fidelity, unstructured-grid-based Navier–Stokes solver. This paper presents the results for the F/A-18E and F-16C configurations. Part II[1] presents similar results for the AV-8B and F/A-18C aircraft configurations.

The objectives of the present study are first listed, followed by a description of the computational method used, as well as its validation. An analysis of the computational results is then presented, and a set of figures of merit (FOMs) are developed against which to measure future aircraft configurations. Finally, important conclusions from the study are presented.

Presented as Paper 2003-0746 at the AIAA 41st Aerospace Sciences Meeting, Reno, NV, 6–9 January 2003; received 3 June 2003; revision received 4 June 2003; accepted for publication 27 October 2003.

*Senior Research Engineer, Configuration Aerodynamics Branch. Associate Fellow AIAA.
†Aerospace Engineer. Senior Member AIAA.

Objectives of the Study

The first objective of the present study was to develop a validated CFD procedure, based on existing unstructured grid-based steady-state CFD technology, for evaluating aircraft designs for AWS. The second objective was to analyze the underlying flow physics that might be responsible for AWS. The final aim was to arrive at static figures of merit as well as recommendations that can be used to screen future aircraft designs for AWS.

Computational Method

All of the computations presented in this paper were carried out using the NASA Langley Research Center developed TetrUSS suite of codes. TetrUSS[2] is a complete flow analysis system based on unstructured, tetrahedral grids. The Navier–Stokes grids were generated, and grid quality improvements accomplished using the component codes VGRIDns[3] and POSTGRIDns, respectively.

The flow solutions were obtained using the TetrUSS flow solver component USM3Dns.[4] This is a three-dimensional, tetrahedral, cell-centered, finite volume, Euler and Navier–Stokes flow solver. In USM3Dns, the inviscid flux quantities are computed across each cell face using Roe's flux difference splitting. Spatial discretization is accomplished by a novel reconstruction process, which is based on an analytical formulation for computing solution gradients within tetrahedral cells. The solution is advanced to a steady-state condition by an implicit backward-Euler time-stepping scheme. Flow turbulence effects are modeled by the Spalart–Allmaras one-equation model. USM3Dns can be run in either a full viscous or a wall-functions mode. All of the calculations in the present study were performed using the full viscous mode. USM3Dns runs on massively parallel computers and on clusters of personal computers. Although a single-processor version is available for a variety of computing platforms, the parallel version[5] is the code of choice because it enables a rapid turnaround for large problems.

Aircraft Configurations

Two aircraft configurations were selected for examination related to AWS for this study: a preproduction F/A-18E configuration,

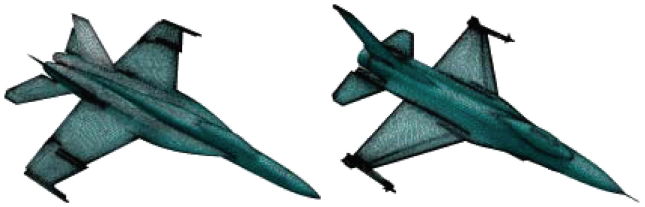

F/A-18E F-16C

Fig. 1 Surface grid for F/A-18E and F-16C configurations.

which showed AWS tendencies during early flight tests, and an F-16C configuration that exhibited no AWS tendencies in its normal operational regime. Because the CFD code was calibrated using experimental data, an attempt was made to closely reproduce as many of the geometric details of the wind-tunnel test model as practical including the wing-tip missile and its attachment hardware as well as flow through ducts representing the engine flow path. Only one side of the symmetric aircraft configuration was modeled, utilizing a plane-of-symmetry boundary condition along the aircraft centerline. The grid resolution used in the CFD study was sufficient to provide a grid spacing of $y^+ = 1$ right next to the body surface based on the wind-tunnel test Reynolds number.

The F/A-18E configuration had a flap setting of 10 deg/10 deg/5 deg—LE /TE/Aileron deflections, respectively—and has been designated as F/A-18E, 10/10/5 in this paper. The unstructured, viscous grid consisted of 3,786,448 tetrahedral cells and 654,840 points. The F-16C configuration modeled has a designation of block 25 to distinguish it from other configurations of the same airplane with small geometrical differences. The configuration had 0-deg deflections for both the leading-edge and trailing-edge flaps. The grid had 6,929,816 tetrahedral cells and 1,205,202 points. Figure 1 shows triangulated surfaces for both configurations. Although the full aircraft configurations are shown in the picture, the CFD study used only half-span configurations, as already stated.

Calibration of the Computer Code

The unstructured grid-based Navier–Stokes solver, USM3Dns, was first calibrated by comparing the CFD force and moment data against wind-tunnel results obtained during companion studies of the AWS program. For the F-16C, block 25 configuration, the CFD data were compared against Veridian (formerly CALSPAN) 8-FT transonic tunnel test T05-590 and NASA Langley Research Center (LaRC) 16-FT Transonic wind-tunnel tests. The comparisons were made for a freestream Mach number of 0.8 at a series of angles of attack α from 6.0 to 16.0 deg. Although the two tests were run at slightly different unit Reynolds number (Reynolds number per foot of 2.5×10^6 for the Veridian test vs 3.63×10^6 for the LaRC test), the CFD was run to match that of the Veridian data. The parallel version of USM3Dns was run on a SGI Origin 3000 parallel computer using 48 processors at a time. Each of the solutions required about 10 GB of memory and a total of about 2500 CPU hours (48 processors $\times$ 54 h) each. For each run, a stringent convergence criterion was used, whereby the solutions were run until changes in the integrated lift coefficient was less than 1.0×10^6 per iteration, that is, a change of less than 0.0005 over 500 iterations. Another convergence criterion used was no noticeable change in surface C_p distribution at selected span stations on the wing of the aircraft over 500 iterations. For the most part, these two criteria amounted to a reduction in global flow residuals (L2 norm) of about five orders of magnitude and required between 3000 and 10,000 iterations, depending upon the flow initialization and the extent of flow separation. In Fig. 2, computed values of the integrated lift, drag, and pitching moment are compared with the experimental data from the two wind-tunnel tests. Not only do the lift coefficient C_L and the pitching-moment coefficient C_m compare well with the experimental data, the drag coefficient C_D also matches well, which is normally difficult to compute accurately. Vertical scales have been suppressed here, and in all subsequent X-Y plots, in compliance with restriction placed by the U.S. Department of Defense.

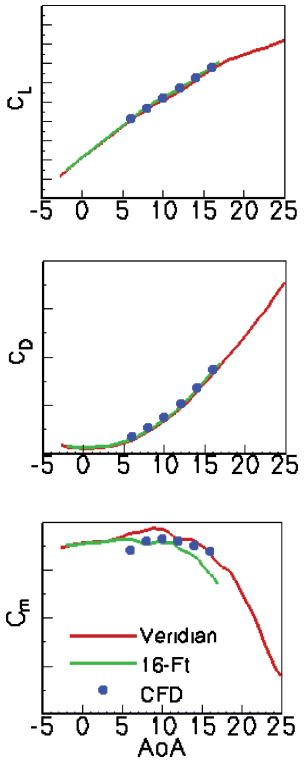

Fig. 2 CFD-experiment comparison for F-16C (block 25) configuration.

This excellent agreement seen in Fig. 2 testifies to the accuracy of the computational method including the adequacy of the grid, the turbulence model, and the convergence criteria used. The experimental data from the two tunnels match closely although both were obtained at slightly different Reynolds numbers. This not only shows the repeatability of the experiments but also a negligible effect of Reynolds number over this small range.

As a further calibration of the code, the CFD data for the F/A-18E configuration are compared against the wind-tunnel Test 523 (Re/Ft. $= 3.8 \times 10^6$) data from the NASA Langley's 16-FT transonic tunnel. Details of this test can be found in Refs. 6 and 7. As reported in these references, the model experienced severe vibrations at transonic conditions believed to be caused by the unsteady movement of shocks on the upper surface of the wing. Because of the unsteady nature of the flow, several repeat runs were made for the transonic conditions in order to obtain an average value during these dynamic conditions. The comparisons in Figs. 3 and 4 show steady-state CFD data plotted against an average (A) of the wind-tunnel test data. In addition, the unsteadiness of the experimental data is quantified by superimposing $\pm$ two times the standard deviation σ at each α. In Fig. 3 the C_L and C_m are compared for a freestream Mach number of 0.9. Both compare reasonably well except that the CFD shows a sharper break in both C_L and C_m at $\alpha = 9.5$ deg and that the predicted lift is slightly higher. Although the vertical scale is not shown on these plots because of the restrictions just mentioned, the discrepancy in C_L is less than 10%.

Similar comparisons made for Mach $= 0.8$, in Fig. 4, show that although the agreement with the lift coefficient is much better the predicted C_m is higher. A number of alternative studies, including a grid refinement and use of a different flow solver, were conducted to understand the discrepancy in C_m, but did not show much improvement. A companion study reported in Ref. 8 shows improved comparison by using a supersonic-transport (SST) turbulence model with the COBALT flow solver. USM3Dns at this time, however, does not have a tested SST model in the code, and hence the stated discrepancy could not be examined further.

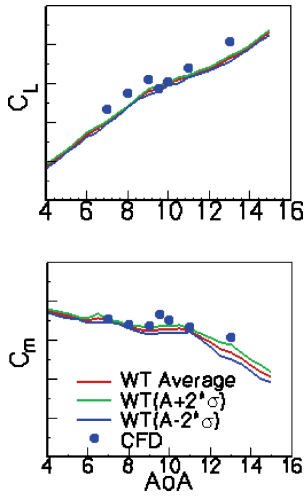

Fig. 3 CFD-experiment comparison for F/A-18E, 10/10/5 configuration; $M = 0.9$.

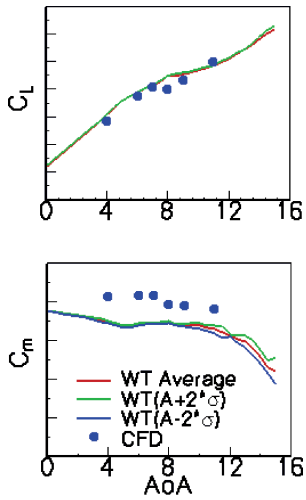

Fig. 4 CFD-experiment comparison, F/A-18E, 10/10/5 configuration; $M = 0.8$.

Analysis of Computational Results

The main aim of the present work is to understand the difference in flow physics between the two configurations studied. It is known, from an analysis of some historical data[8] as well as from wind-tunnel studies conducted during this program, that AWS is a result of one of the wings of an aircraft experiencing a sudden loss of lift resulting from a sudden movement of separation caused by a small change in the angle of attack. Thus, an AWS event is characterized by a change in the lift-curve slope over a small change in α. The CFD results presented in the earlier section show such a behavior for the preproduction F/A-18E configuration at $\alpha = 9.5$ and 8.0 deg for freestream Mach numbers of 0.9 and 0.8, respectively. In contrast, the F-16C results shown in Fig. 2 display a smooth, almost linear variation. It is, therefore, implied that important FOMs characterizing AWS can be developed by studying the differences in the simulated physical phenomena associated with these two aircraft.

In light of these observations, the CFD results are analyzed for the wing upper surface C_p distribution and the behavior of flow separation as the angle of attack is increased for a fixed freestream Mach number. Figure 5 shows a collage of such plots, one for each angle, for the benign F-16C configuration. For each frame, the right side shows the surface C_p distribution while on the left side surface contours of negative streamwise velocity are displayed, the extent of which represents flow separation on the surface.

For lower angles of attack, only a narrow portion near the wing leading edge shows flow separation. As the angle of attack increases,

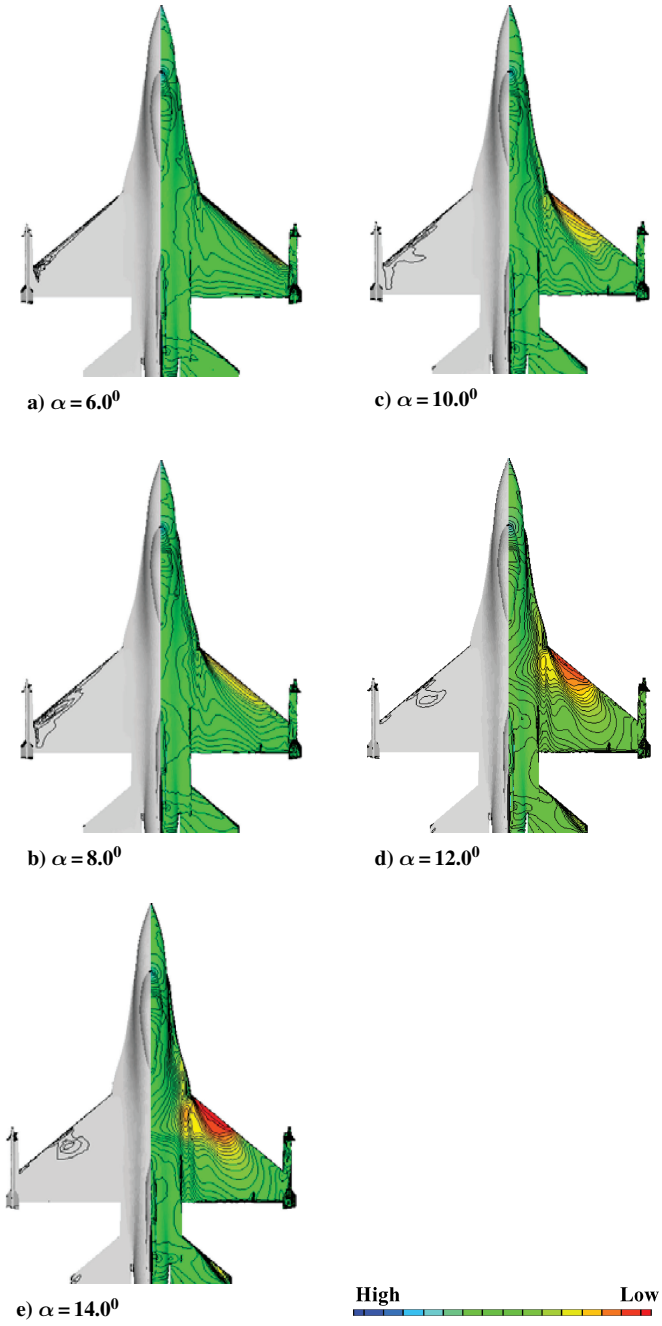

Fig. 5 C_p distribution and separation progression on the wing upper surface for F-16C at $M = 0.8$.

the separation region slowly spreads further downstream, but the lift on the configuration keeps increasing in part because of an increased contribution from a stronger leading-edge-extension vortex.

A similar collage is shown in Fig. 6 for the F/A-18E configuration at a freestream Mach number of 0.8. Unlike the F-16C, here even at lower angles there is a strong shock present near the outboard portion of the wing resulting in a small region of boundary-layer separation as shown on the left part of the Fig. 6a. As the angle of attack increases, the shock moves forward, along with an increase in the separated region from downstream of the shock extending all of the way to the wing trailing edge. Observe that this behavior suddenly changes as the angle of attack is increased from 7.0 to 8.0 degs, where the separation region abruptly spreads from about 30% of the chord all of the way to the leading edge of the wing. This sudden change in the separation behavior is associated with a sudden drop in the overall lift for the wing. If this happens asymmetrically, the aircraft can experience a large rolling moment and hence AWS.

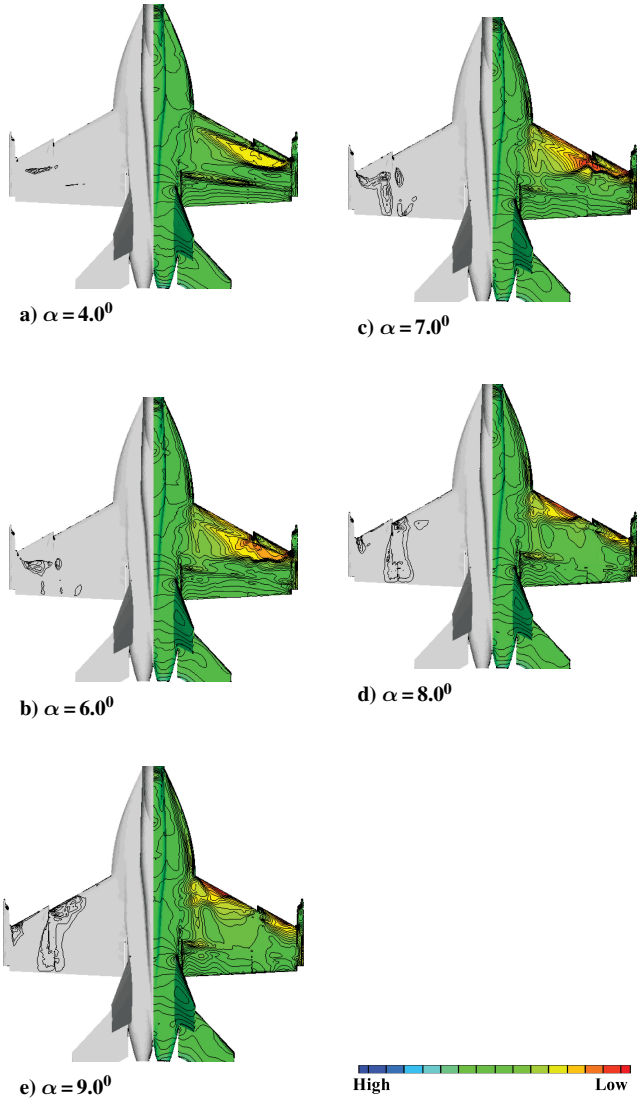

Fig. 6 C_p distribution on the wing upper surface for F/A-18E, 10/10/5 at $M = 0.8$.

In summary, the abrupt change in the extent of separation on the wing upper surface resulting from a small change in angle of attack can be indicative of AWS on a configuration.

Figures of Merit

The steady-state computational results were further analyzed to arrive at aerodynamic indicators against which to measure future configurations for the presence of AWS. As shown for the F/A-18E aircraft, such indicators have to be related to changes in the separation pattern on the lifting wing. Local separation anywhere on a wing should result in a corresponding decrease in lift contribution of that wing panel to the overall lift. Thus, a study of the spanwise distribution of sectional lift can be an indicator of AWS susceptibility. In addition, depending upon the distance of the separated region from the aircraft centerline there will a corresponding decrease in that wing panel's contribution to the total rolling moment of the configuration. Traditionally, wind-tunnel experiments are conducted on full aircraft configurations. Thus, the rolling moment measured during a wind-tunnel test has contribution of opposite sign from the left and the right wings. Hence the effect of separation on only one of the wings is harder to quantify by measuring the rolling moment. As an alternative, the wind-tunnel programs use wing-root bending moment (WRBM) measured by one or more gauges located near the wing root to quantify the effect of separation on the wing.

Based on these considerations, two aerodynamic indicators or figures of merit have been proposed and are tested in this study; 1) the spanwise distribution of the wing sectional lift coefficient and its rate of change with respect to α and 2) the change in the WRBM as α changes.

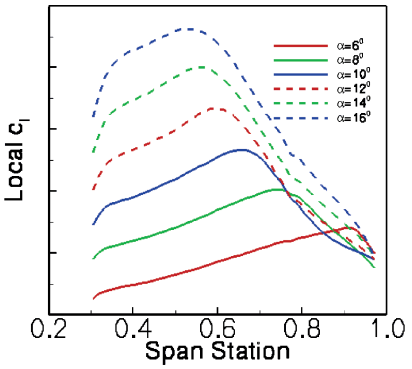

Fig. 7 Spanwise distribution of sectional c_l for F-16C configuration at $M = 0.8$.

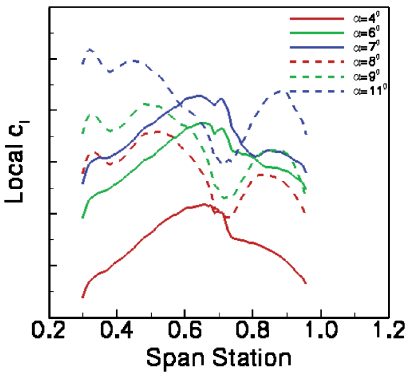

Fig. 8 Spanwise distribution of sectional c_l for F/A-18E configuration at $M = 0.8$.

Spanwise Distribution of Sectional Lift

The sectional lift coefficient is defined as the integrated value of the upper and lower surface C_p distribution at a wing span station, where C_p is obtained from the CFD solution:

$$c_l = \int_0^1 \Delta C_P \, \mathrm{d}\left(\frac{x}{c}\right)$$

The spanwise variation is then obtained by calculating the preceding integral at several spanwise locations. Such a distribution is shown in Figs. 7 and 8 for F-16C and F/A-18E, respectively.

As shown in Fig. 7 for the F-16C configuration, with an increase in the angle of attack the lift contribution of the in-board wing panel continues to increase, whereas that of the outer panel either decreases or remains constant because of the spread of the upper surface separation. But the overall lift increases in a smooth fashion. On the other hand, for the F/A-18E configuration as shown in Fig. 8 the spanwise lift distribution changes dramatically between $\alpha = 7.0$ and 8.0 deg as a result of the sudden movement of separation all the way to the wing leading edge signifying an AWS event.

Contrasting Fig. 8 with Fig. 7, it is obvious that the spanwise distribution of sectional lift distribution across the wing through the stall process can give a quick glance at how abrupt or smooth the stall process is and can form an important FOM that can be easily evaluated.

Rate of Change of Sectional Lift

Although the spanwise distribution of sectional lift can give an indication of AWS, a more definitive insight can be gained by examining its quantitative rate of change with respect to α. Figures 9 and 10 show $\mathrm{d}c_l/\mathrm{d}\alpha$ plotted against the span station for the F-16C and F/A-18E, respectively. Although the vertical scale is not shown,

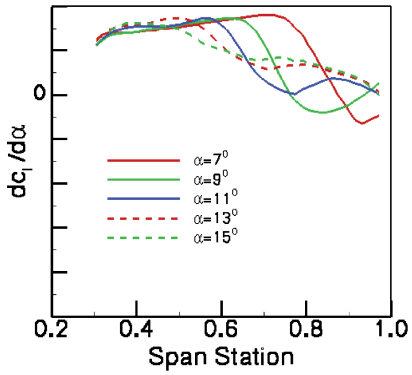

Fig. 9 Spanwise distribution of $dc_l/d\alpha$ for F-16C configuration at $M = 0.8$.

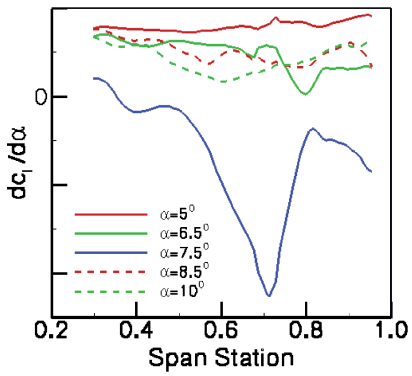

Fig. 10 Spanwise distribution of $dc_l/d\alpha$ for F/A-18E configuration at $M = 0.8$.

both figures have been plotted using the same vertical scale, and thus show the relative "strength" or abruptness of the wing stall. As shown in Fig. 9 for the F-16C, there is a smooth variation of $dc_l/d\alpha$ across the span, whereas for the F/A-18E the large "dip" in Fig. 10 around span station 70%, for the curve labeled $\alpha = 7.5$ deg, corresponds to the AWS phenomenon observed as the α changes from 7.0 to 8.0 deg, as shown in Fig. 4.

Compared to the spanwise distribution of sectional lift, the additional information that plots in Figs. 9 and 10 provide is the spanwise location where largest lift loss occurs. Thus, giving the location where design modification efforts need to be concentrated to alleviate AWS.

Wing-Root Bending Moment

Loss of local lift as a result of flow separation causes corresponding loss of rolling moment as explained earlier. Based on correlations with wind-tunnel and flight-test data, it has been shown that abrupt wing stall can occur when the slope of the WRBM vs α curve changes sign.[9] Thus, a study of the WRBM can be used as a potential FOM. This is shown in Fig. 11, where the WRBM extracted from the CFD solutions is plotted against α for the two aircraft configurations studied here. The change in the slope between $\alpha = 7.0$ and 8.0 deg for the F/A-18E clearly shows the AWS event. All of the data on in this figure are CFD data; symbols are shown only for clarity.

Half-Plane Rolling Moment

Although calculation of WRBM from CFD studies is straightforward, it does involve additional computations of force integration not normally done as part of a routine CFD calculation. Because normally a CFD study is performed on only half of a symmetrical configuration to save computational resources and because the rolling moment calculated for half-configuration [termed half-plane rolling moment, (HPRM)] does not involve additional processing, it is worthwhile to see if it can be used as a potential FOM. This is

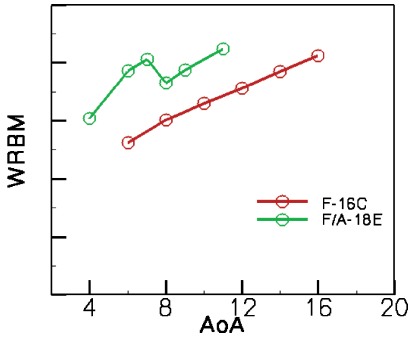

Fig. 11 Comparison of wing-root bending moment from CFD data at $M = 0.8$.

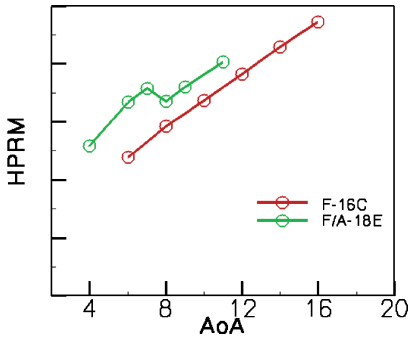

Fig. 12 Comparison of half-plane rolling moment from CFD data at $M = 0.8$.

shown in Fig. 12, where HPRM is compared for the two configurations. The similarity of the curves in Figs. 11 and 12 thus establishes HPRM from half-configuration CFD analyses as a viable FOM for any AWS study. Additionally, as has been shown in Part II of this study (Ref. 1), at times the HPRM vs α curve is a little clearer indicator of the wing stall compared to a lift curve.

In summary, as shown, the potential FOMs for any abrupt-wing-stall study using steady CFD are as follows: 1) the spanwise variation of sectional lift and its rate of change with respect to α, and 2) the slope change in the C_L, WRBM (or equivalently HPRM) vs α.

Conclusions

A validated computational-fluid-dynamics (CFD) procedure based on an unstructured grid method and steady-state Navier–Stokes solutions has been developed for evaluating AWS behavior of aircraft. A set of static figures of merit (FOM) has been developed by analyzing CFD results and is shown to be consistent with flight results for the two aircraft analyzed. The static FOMs include slope change in the C_L and wing-root bending mement (WRBM) vs α as well as an abrupt change in the spanwise distribution of local lift. In addition, the half-plane rolling moment (HPRM) calculated from configuration CFD is shown to provide the same information in predicting AWS as the WRBM, thus establishing HPRM as a viable FOM for steady state, half-configuration CFD studies.

Results of these and other companion CFD studies conducted under the AWS program have been used to prepare CFD-based recommendations[10] that can be used to evaluate future configurations for AWS susceptibility or lack thereof.

Acknowledgments

This work was supported by the NASA Aerospace Systems Concepts to Test program, Naval Air Systems Command, and the Office of Naval Research. The authors would like to thank Edward Parlette of Vigyan, Inc., for grid generation help and Jonathan Nehrbass, a co-op student in the Configuration Aerodynamics Branch at NASA Langley Research Center for graphics related help.

References

[1]Chung, J., and Parikh, P., "A Computational Study of the Abrupt Wing Stall (AWS) Characteristics for various Fighter Jets: Part II, AV-8B and F/A-18C," AIAA Paper 2003-0747, Jan. 2003.

[2]Frink, N. T., Pirzadeh, S., Parikh, P., Pandya, M. J., and Bhat, M. K., "The NASA Tetrahedral Unstructured Software System (TetrUSS)," *The Aeronautical Journal*, Vol. 104, No. 1040, 2000, pp. 491–499.

[3]Pirzadeh, S., "Three-Dimensional Unstructured Viscous Grids by the Advancing Layers Method," *AIAA Journal*, Vol. 34, No. 1, 1996, pp. 43–49.

[4]Frink, N. T., "Tetrahedral Unstructured Navier–Stokes Method for Turbulent Flows," *AIAA Journal,* Vol. 36, No. 11, 1998, pp. 1975–1982.

[5]Bhat, M. K., and Parikh, P., "Parallel Implementation of an Unstructured Grid-Based Navier–Stokes Solver," AIAA Paper 99-0663, Jan. 1999.

[6]McMillin, N., Hall, R., and Lamar, J., "Understanding Abrupt Wing Stall with Experimental Methods (Invited)," AIAA Paper 2003-0591, Jan. 2003.

[7]Schuster, D., and Byrd, J., "Transonic Unsteady Aerodynamics of the F/A-18E at Conditions Promoting Abrupt Wing Stall," *Journal of Aircraft*, Vol. 41, No. 3, 2004, pp. 485–492.

[8]Forsythe, J. R., and Woodson, S. H., "Unsteady Computations of Abrupt Wing Stall Using Detached-Eddy Simulation," *Journal of Aircraft*, Vol. 42, No. 3, 2005, pp. 606–616.

[9]Green, B. E., and Ott, J. D., "F/A-18C to E Wing Morphing Study for the Abrupt-Wing-Stall Program," *Journal of Aircraft*, Vol. 42, No. 3, 2005, pp. 617–626.

[10]Woodson, S. H., Green, B. E., Chung, J. J., Grove, D. V., Parikh, P. C., and Forsythe, J. R., "Recommendations for Computational-Fluid-Dynamics Procedures for Predicting Abrupt Wing Stall," *Journal of Aircraft*, Vol. 42, No. 3, 2005, pp. 627–633.